Stability of Leapfrog Constant-Coefficients Semi-Implicit Schemes for the Fully Elastic System of Euler Equations: Flat-Terrain Case

P. BÉNARD

Centre National de Recherches Météorologiques, Météo-France, Toulouse, France

R. LAPRISE

Université du Québec à Montréal, Montréal, Québec, Canada

J. VIVODA

Slovak Hydrometeorological Institute, Bratislava, Slovakia

P. SMOLÍKOVÁ

Czech Hydrometeorological Institute, Prague, Czech Republic

(Manuscript received 9 April 2003, in final form 17 September 2003)

ABSTRACT

The stability of semi-implicit schemes for the hydrostatic primitive equations system has been studied extensively over the past 20 yr, since this temporal scheme and this system represented a standard for NWP. However, with the increase of computational power, the relaxation of the hydrostatic approximation through the use of nonhydrostatic fully elastic systems is now emerging for future NWP as an attractive solution valid at any scale. In this context, several models employing the so-called Euler equations together with a constant-coefficients semi-implicit time discretization have already been developed, but no solid justification for the suitability of this algorithmic combination has been presented so far, especially from the point of view of robustness.

The aim of this paper is to investigate the response of this system/scheme in terms of stability in presence of explicitly treated residual terms, as it inevitably occurs in the reality of NWP. This study is restricted to the impact of thermal and baric residual terms (metric residual terms linked to the orography are not considered here). It is shown that, conversely to what occurs with hydrostatic primitive equations, the choice of the prognostic variables used to solve the system in time is of primary importance for the robustness with Euler equations. For an optimal choice of prognostic variables, unconditionally stable schemes can be obtained (with respect to the length of the time step), but only for a smaller range of reference states than in the case of hydrostatic primitive equations. This study also indicates that (i) vertical coordinates based on geometrical height and on mass behave similarly in terms of stability for the problems examined here, and (ii) hybrid coordinates induce an intrinsic instability, the practical importance of which is, however, not completely elucidated in the theoretical context of this paper.

1. Introduction

In their most general definition, semi-implicit (SI) schemes consist of an arbitrary separation of the evolution terms of any dynamical system between some linear terms, treated implicitly, and nonlinear residuals (NL residuals hereafter), treated explicitly. In meteorology, depending on the nature of the implicitly treated terms, three main types of SI schemes can be distinguished. The coefficients of these linear terms may be (i) constant both in time and horizontally; (ii) constant in time only; and (iii) nonconstant.

The first approach was initially introduced for meteorological applications by Robert et al. (1972) and has been extensively used in numerical weather prediction (NWP) since the solution of the resulting implicit system requires only basic techniques. However, because of large NL residuals, the stability of these schemes is not formally guaranteed, especially for long time steps.

The second and third approaches require more sophisticated techniques for solving the resulting implicit system, but they allow a significant reduction of the magnitude of the explicitly treated residuals and, hence, a potentially better stability.

Corresponding author address: Pierre Bénard, CNRM/GMAP, 42, Avenue G. Coriolis, F-31057 Toulouse Cedex, France.
E-mail: pierre.benard@meteo.fr

In the present paper, the term ''constant-coefficients SI schemes'' exclusively refers to the above first category of SI schemes, and only these schemes are considered in all the following, unless expressly mentioned.

Historically, SI schemes were first applied in NWP for solving the hydrostatic primitive equations (HPEs) system, and extensive stability studies have been carried out with this system. Simmons et al. (1978, hereafter SHB78) investigated the practical stability of HPEs with the three-time-level (3-TL) leapfrog constant-coefficients SI scheme in the terrain-following pressure-based σ coordinate. To do so, they examined the effect of the leading NL residual terms on the stability when the SI reference temperature deviates from the actual temperature. They showed that, in the particular case where the complete model operator and the linearized SI operator have the same eigenfunctions, the stability can be studied analytically. In the more general case, when this latter condition is not fulfilled, Coté et al. (1983, hereafter CBS83) showed that the stability can still be assessed, but at the price of a ''numerical analysis'' that can be performed only in the space-discretized context; the stability analysis then becomes an eigenvalue problem in a generalized state-vector space where the whole space- and time-discretized model acts as a so-called ''amplification matrix.'' The salient result of SHB78 was that a warm isothermal choice for the SI reference temperature profile resulted in a more stable scheme than when using climatological profiles for the SI reference state, a rule that has been widely followed in practical NWP applications. The two methods proposed by SHB78 and CBS83 (analysis in simplified cases and numerical analysis in the general case) have been adopted by most of subsequent studies on the SI scheme stability. CBS83 showed that, for the finite-element vertical discretization of a 3-TL HPE model in σ coordinate, the SI reference-state static stability had to be larger than half the actual one, in order to achieve stability, which explains and generalizes the previous results by SHB78. Simmons and Temperton (1997, hereafter ST97) have extended the study of SHB78 to extrapolating two-time-level (2-TL) SI schemes still in the HPE system but for the more general hybrid-pressure terrain-following η coordinate (in η coordinate, the surface pressure in the SI reference state also has to be considered for the stability of the SI scheme).

However, with the increasing resolutions allowed by faster computers, nonhydrostatic (NH) models are now accessible to NWP, thus avoiding the limitations associated with the hydrostatic assumption. However, the aim for NWP models should be to achieve the relaxation of the hydrostatic approximation while keeping the same degree of efficiency as the former HPE SI semi-Lagrangian systems. This pleads in favor of attempting to extend the SI technique to the new generation of nonhydrostatic semi-Lagrangian models. Among the possible NH systems, the fully elastic Euler equations (EE) system is generally advocated for several reasons, including the possibility of building a ''universal'' atmospheric model whose dynamical kernel is valid for all scales used by the meteorological community.

Several models using the EE system with a constant-coefficients SI scheme have been recently developed (Tanguay et al. 1990; Laprise et al. 1995; Semazzi et al. 1995; Bubnová et al. 1995, hereafter BHBG95; Caya and Laprise 1999), but the stability of such a combination has not yet been studied in detail. Tanguay et al. (1990) examined the stability of the tangent-linear version of their model around the SI reference state (i.e., in the absence of nonlinear terms). Not surprisingly, they found that the system is unconditionally stable, since this follows from a general property of any purely linear SI physical system. However, the experience accumulated with former HPE systems clearly indicates that some care must be taken when (explicitly treated) nonlinear terms are present. Moreover, there is no objective reason to expect an intrinsically more robust behavior of the SI EE system compared to the SI HPE system. Especially, when increasing the resolution to mesoscales, terms associated with the orographic forcing or with physical processes could have an increasingly stringent impact on the stability, due to their increased contribution in the total evolution. In BHBG95, we reported an unstable behavior for the EE system with the SI time discretization, and this problem was solved in the Eulerian context through the iteration of a part of the NL residual terms. However, the unstable behavior reappeared when the resolution was refined or when the time step was increased, as allowed by the implementation of a semi-Lagrangian scheme. This prompted us to undertake this study. A general formalism for studying the stability of various time discretizations (including the SI scheme) and equation systems (including the EE system) is presented in Bénard (2003, B03 hereafter). This general method is applied here to the case of the 3-TL SI scheme for the EE system with flat orography, in order to show the essential role played by the choice of prognostic variables in the robustness of the system.

2. Framework of analyses

In this paper (except in appendix B), the EE are cast in the pure unstretched terrain-following coordinate σ, which can be classically derived from the mass-based hydrostatic-pressure coordinate π (Laprise 1992) through $\sigma = (\pi/\pi_s)$, where π_s is the hydrostatic surface pressure. The σ coordinate examined here is a particular case of the general stretched hybrid-pressure terrain-following coordinate η of BHBG95. However, the use of the σ coordinate is advantageous for the theoretical analysis since it possesses a much simpler vertical metrics. Starting from the general η formalism, the equations for the σ coordinate can be obtained by setting the arbitrary $A(\eta)$ and $B(\eta)$ functions in Eq. (9) of BHBG95 as follows:

$$A(\eta) = 0, \tag{1}$$

$$B(\eta) = \eta \equiv \sigma. \tag{2}$$

In all the discussions in this paper, the flow is assumed adiabatic inviscid and frictionless in a nonrotating perfect-gas dry atmosphere with a Cartesian coordinate system. In these conditions, the complete set of Euler equations can be easily derived from BHBG95 Eqs. (1)–(8) with the same standard notations (for nonstandard notations see appendix A). The system in σ coordinate writes

$$\frac{d\mathbf{V}}{dt} + RT\frac{\boldsymbol{\nabla} p}{p} + \frac{1}{\pi_s}\frac{\partial p}{\partial \sigma}\boldsymbol{\nabla}\phi = 0, \tag{3}$$

$$\frac{dw}{dt} + g\left(1 - \frac{1}{\pi_s}\frac{\partial p}{\partial \sigma}\right) = 0, \tag{4}$$

$$\frac{dT}{dt} - \frac{RT}{C_v}D_3 = 0, \tag{5}$$

$$\frac{dp}{dt} + \frac{C_p}{C_v}pD_3 = 0, \tag{6}$$

$$\frac{\partial q}{\partial t} + \int_0^1 (\mathbf{V}\cdot\boldsymbol{\nabla} q + \boldsymbol{\nabla}\cdot\mathbf{V})\, d\sigma = 0, \tag{7}$$

where the three-dimensional divergence is given by

$$D_3 = \boldsymbol{\nabla}\cdot\mathbf{V} + \frac{p}{\pi_s RT}\left(\frac{\partial \mathbf{V}}{\partial \sigma}\right)\cdot\boldsymbol{\nabla}\phi - g\frac{p}{\pi_s RT}\frac{\partial w}{\partial \sigma}, \tag{8}$$

and the geopotential horizontal gradient is

$$\boldsymbol{\nabla}\phi = \boldsymbol{\nabla}\phi_s + R\int_\sigma^1 \boldsymbol{\nabla}\left(\frac{\pi_s T}{p}\right) d\sigma'. \tag{9}$$

We note $q = \ln(\pi_s)$, p is the true pressure, and w is the vertical velocity. The theoretical analysis of the stability of nonlinear systems such as (3)–(7) is not possible in the most general conditions and requires some simplifications in order to become algebraically tractable. For the analyses presented here, we use the same method and notations as in B03, which is basically a generalization of the method proposed by SHB78. In symbolic notations, the equations of the system to be solved can be written as

$$\frac{\partial \mathcal{X}}{\partial t} = \mathcal{M}(\mathcal{X}), \tag{10}$$

where $\mathcal{X}$ is the state variable, and $\mathcal{M}$ is the full model operator containing only spatial dependencies on $\mathcal{X}$. For the definition of the SI scheme, as usually done in NWP, an SI reference state $\mathcal{X}^*$ is chosen, and the system $\mathcal{M}$ is linearized around $\mathcal{X}^*$, resulting in a linear operator noted $\mathcal{L}^*$. The 3-TL SI time discretization writes

$$\frac{\mathcal{X}^+ - \mathcal{X}^-}{2\Delta t} = [\mathcal{M}(\mathcal{X}^0) - \mathcal{L}^*\cdot\mathcal{X}^0] + \mathcal{L}^*\cdot\left(\frac{\mathcal{X}^+ + \mathcal{X}^-}{2}\right), \tag{11}$$

where the superscript $(-, 0, +)$ indicates variables at time $(t - \Delta t)$, t, and $(t + \Delta t)$, respectively, where Δt is the length of the time step. The stability of the model is then conditioned by the structure of the NL residual $(\mathcal{M} - \mathcal{L}^*)$.

For the purpose of analyses, the flow is assumed to consist of small perturbations around a steady basic state $\overline{\mathcal{X}}$. Hence $\mathcal{M}(\overline{\mathcal{X}}) = (\partial\overline{\mathcal{X}}/\partial t) = 0$, and the full model evolution $\mathcal{M}$ can be described by $\overline{\mathcal{L}}$, the linear-tangent operator of $\mathcal{M}$ around $\overline{\mathcal{X}}$.

The 3-TL SI time-discretized equation then becomes

$$\frac{\mathcal{X}^+ - \mathcal{X}^-}{2\Delta t} = (\overline{\mathcal{L}} - \mathcal{L}^*)\cdot\mathcal{X}^0 + \mathcal{L}^*\cdot\left(\frac{\mathcal{X}^+ + \mathcal{X}^-}{2}\right), \tag{12}$$

which represents the equation to be solved in the simplified framework examined here. Note that $\overline{\mathcal{X}} \neq \mathcal{X}^*$, and hence $\overline{\mathcal{L}} \neq \mathcal{L}^*$, thus giving rise to explicit contributions in (12). The other simplifications adopted for the present analyses (as well as in SHB78) consist of assuming that both basic and SI reference states are resting, isothermal, and hydrostatically balanced, with a uniform (plateau) orography.

As a consequence, in hydrostatic-pressure-based coordinates, the $\overline{\mathcal{X}}$ and $\mathcal{X}^*$ states are simply characterized by their uniform temperature and hydrostatic-surface-pressure fields, that is, by the pairs of numbers $(\overline{T}, \overline{\pi}_s)$ and (T^*, π_s^*), respectively. Finally, the domain is assumed two-dimensional (in a vertical plane), with x as horizontal coordinate. Examining the stability of the numerical system in this highly simplified context of course leads to an overestimation of the stability compared to what can be expected for more complex flows with a fully nonlinear model. However, if a scheme is found unstable here, it will have little chance of being applicable in practice.

3. Impact of the SI reference pressure

In this section, we examine the SI scheme for EE when the actual hydrostatic surface pressure $\overline{\pi}_s$ deviates from its SI reference counterpart π_s^*, everything else being equal for the two states. Hence, in this section the basic $\overline{\mathcal{X}}$ and reference $\mathcal{X}^*$ states are characterized by $(\overline{T} \equiv T^*, \overline{\pi}_s)$ and (T^*, π_s^*), respectively. The linearized equations are derived from (3)–(7) or from Eqs. (13)–(21) of BHBG95, with the following set of prognostic variables—horizontal divergence D, temperature T, $q = \ln(\pi_s)$, and the following two nonhydrostatic variables as in BHBG95:

$$\hat{\mathcal{P}} = \frac{p - \pi}{\pi^*}, \tag{13}$$

$$\hat{d} = -g\frac{\pi^*}{m^*RT^*}\frac{\partial w}{\partial \eta}, \tag{14}$$

where $\pi^*(\eta)$ is the SI reference pressure profile, and $m^*(\eta) = (d\pi^*/d\eta)$. In σ coordinate, these variables become

$$\hat{\mathcal{P}} = \frac{p - \pi}{\sigma\pi_s^*}, \tag{15}$$

$$\hat{d} = -g\frac{\sigma}{RT^*}\frac{\partial w}{\partial \sigma}. \tag{16}$$

The $\overline{\mathcal{L}}$ system then writes

$$\frac{\partial D}{\partial t} = -R\mathcal{G}\nabla^2 T + RT^*\left[\frac{\pi_s^*}{\overline{\pi}_s}\right](\mathcal{G} - I)\nabla^2\hat{\mathcal{P}} - RT^*\nabla^2 q, \tag{17}$$

$$\frac{\partial \hat{d}}{\partial t} = -\frac{g^2}{RT^*}\left[\frac{\pi_s^*}{\overline{\pi}_s}\right]\tilde{\delta}(\tilde{\delta} + I)\hat{\mathcal{P}}, \tag{18}$$

$$\frac{\partial T}{\partial t} = -\frac{RT^*}{C_v}(D + \hat{d}), \tag{19}$$

$$\frac{\partial \hat{\mathcal{P}}}{\partial t} = \left[\frac{\overline{\pi}_s}{\pi_s^*}\right]\mathcal{S}D - \frac{C_p}{C_v}\left[\frac{\overline{\pi}_s}{\pi_s^*}\right](D + \hat{d}), \tag{20}$$

$$\frac{\partial q}{\partial t} = -\mathcal{N}D, \tag{21}$$

where the notations follow BHBG95 (see also appendix A for the meaning of vertical operators I, $\mathcal{G}$, $\mathcal{S}$, $\mathcal{N}$, and $\tilde{\delta}$ in σ coordinate).

The SI linear model $\mathcal{L}^*$ can be derived in a similar way except that π_s^* is used instead of $\overline{\pi}_s$: it is then formally identical to $\overline{\mathcal{L}}$, except that the factors in brackets in the above system become equal to 1. As a consequence, the explicitly treated NL residual model ($\overline{\mathcal{L}} - \mathcal{L}^*$) in (12) is nonzero, leading to a potential source of instability resulting from the departure of $\overline{\pi}_s$ from π_s^*.

An alternative formulation can be obtained if the variable $\hat{\mathcal{P}}$ is replaced by a new variable $\mathcal{P}$ defined by

$$\mathcal{P} = \frac{p - \pi}{\pi}. \tag{22}$$

The form of the full nonlinear model $\mathcal{M}$ is modified in such a way that all occurrences of $\hat{\mathcal{P}}$ on the rhs must be replaced by $(\pi/\pi^*)\mathcal{P}$, and the pressure departure equation becomes

$$\frac{d\mathcal{P}}{dt} = \frac{\pi^*}{\pi}\left[\frac{d\hat{\mathcal{P}}}{dt}\right] + \frac{\pi\mathcal{P}}{\pi^*}\frac{d}{dt}\left(\frac{\pi^*}{\pi}\right), \tag{23}$$

where the bracketed term is the rhs of the original prognostic $\hat{\mathcal{P}}$ equation. The last term of (23) is identically zero for the linearized $\overline{\mathcal{L}}$ and $\mathcal{L}^*$ systems. Moreover, the factor (π^*/π) writes $(\pi_s^*/\overline{\pi}_s)$ in the present linearized context in σ coordinate. As a consequence, the new $\overline{\mathcal{L}}$ system writes

$$\frac{\partial D}{\partial t} = -R\mathcal{G}\nabla^2 T + RT^*(\mathcal{G} - I)\nabla^2\mathcal{P} - RT^*\nabla^2 q, \tag{24}$$

$$\frac{\partial \hat{d}}{\partial t} = -\frac{g^2}{RT^*}\tilde{\delta}(\tilde{\delta} + I)\mathcal{P}, \tag{25}$$

$$\frac{\partial T}{\partial t} = -\frac{RT^*}{C_v}(D + \hat{d}), \tag{26}$$

$$\frac{\partial \mathcal{P}}{\partial t} = \mathcal{S}D - \frac{C_p}{C_v}(D + \hat{d}), \tag{27}$$

$$\frac{\partial q}{\partial t} = -\mathcal{N}D. \tag{28}$$

Since this system has no dependency on π_s^*, it is obvious that the SI reference system $\mathcal{L}^*$ will have exactly the same form as $\overline{\mathcal{L}}$ for this set of variables. In fact, it can be seen that using the variables (q, $\mathcal{P}$) and the σ coordinate allows a complete elimination of the SI reference surface pressure π_s^* from the model formulation, in opposition to what occurs when using π_s and/or $\hat{\mathcal{P}}$ as prognostic variables and/or the general hybrid η coordinate. For the new variable $\mathcal{P}$, there is no NL residual terms, and hence no potential source of instability due to the discrepancy between π_s and π_s^* for the examined problem. As a direct consequence, no stability analysis is necessary here to conclude that the variable $\mathcal{P}$ is better suited to the design of an SI scheme than $\hat{\mathcal{P}}$.

Similar algebraic derivations show that for the particular problem examined here, the various possible choices for the prognostic pressure variables fall into two classes:

1) variables leading to potentially unstable SI: p, p/p_0, $p - \pi$, p/π^*, $\hat{\mathcal{P}}$, and
2) variables leading to stable SI: $\ln(p)$, $\ln(p/p_0)$, p/π, $\ln(p/\pi)$, $\mathcal{P}$,

where p_0 is an arbitrary constant. It is worth emphasizing that the above statement holds for height-based coordinates as well as for the mass-based coordinate that was used here (with of course the restriction due to the fact that the variables involving π are not natural with height-based coordinates). These properties follow immediately from the derivation of the corresponding linear system in the same context, for height-based coordinates. From now on, the new variable $\mathcal{P}$ will be used instead of the original variable $\hat{\mathcal{P}}$ used in BHBG95.

4. Impact of the SI reference temperature

In this section, we examine the stability of the SI scheme for EE with the prognostic variables (D, $\hat{d}$, T, $\mathcal{P}$, q) when the basic uniform temperature $\overline{T}$ deviates from the SI reference-state temperature T^*, everything else being equal for the two states. The variable $\hat{d}$ is

still given by (16). As a consequence, the three-dimensional divergence D_3 [(8)] writes for the $\overline{\mathcal{L}}$ system

$$D_3 = D + \frac{T^*}{\overline{T}}\hat{d}, \tag{29}$$

and the direct linearization of the original system yields

$$\frac{\partial D}{\partial t} = -R\mathcal{G}\nabla^2 T + R\overline{T}(\mathcal{G} - \mathcal{I})\nabla^2\mathcal{P} - R\overline{T}\nabla^2 q, \tag{30}$$

$$\frac{\partial \hat{d}}{\partial t} = -\frac{g^2}{RT^*}\tilde{\partial}(\tilde{\partial} + \mathcal{I})\mathcal{P}, \tag{31}$$

$$\frac{\partial T}{\partial t} = -\frac{R\overline{T}}{C_v}\left(D + \frac{T^*}{\overline{T}}\hat{d}\right), \tag{32}$$

$$\frac{\partial \mathcal{P}}{\partial t} = \mathcal{S}D - \frac{C_p}{C_v}\left(D + \frac{T^*}{\overline{T}}\hat{d}\right), \tag{33}$$

$$\frac{\partial q}{\partial t} = -\mathcal{N}D. \tag{34}$$

The $\mathcal{L}^*$ operator is defined in a similar way, simply replacing $\overline{T}$ by T^* in the rhs of the above system.

The method for the stability analysis exactly follows the one proposed in B03, and the reader is invited to refer to this paper for more details on the notations and the algebraic developments. The above system is first shown to fulfill the four conditions (C1–C4) required for making possible the space-continuous analyses with the proposed method. The number of prognostic variable is $P = 4$ in the sense of B03, and the space-continuous state vector is $\mathcal{X} = (\mathcal{X}_1, \ldots, \mathcal{X}_4) = (D, \hat{d}, T, \mathcal{P})$. The linear operator in C1 involves $l_1 = \tilde{\partial}$ applied to (30) and $l_4 = (\tilde{\partial} + \mathcal{I})$ applied to (33) as in section 7a of B03. The condition C2 requires $\overline{T} > 0$, and the normal modes of the system are then

$$\mathcal{X}_j(x, \sigma) = \hat{\mathcal{X}}_j \exp(ikx)\sigma^{(i\nu - 1/2)}, \quad \text{for } j \in (1, \ldots, 4), \tag{35}$$

where $(k, \nu) \in \mathbb{R}$ (note that ν is a nondimensional vertical wavenumber). In this particular case, the four components $(f_1, \ldots, f_4)$ of the shape function f introduced in B03 are identical. The vector function f represents the geometry of any normal mode of the time- and space-continuous system. The verification of C3 and C4 proceeds easily, as in B03; for C3, we have

$$\xi_1 = i\nu - 1/2, \tag{36}$$

$$\xi_4 = i\nu + 1/2, \tag{37}$$

and for C4,

$$\overline{\mu}_{13} = \mu^*_{13} = -k^2 R, \tag{38}$$

$$\overline{\mu}_{14} = k^2 R\overline{T}(i\nu + 1/2), \qquad \mu^*_{14} = k^2 RT^*(i\nu + 1/2), \tag{39}$$

$$\overline{\mu}_{24} = \mu^*_{24} = \left(\nu^2 + \frac{1}{4}\right)\frac{g^2}{RT^*}, \tag{40}$$

$$\overline{\mu}_{31} = -\frac{R\overline{T}}{C_v}, \qquad \mu^*_{31} = \overline{\mu}_{32} = \mu^*_{32} = -\frac{RT^*}{C_v}, \tag{41}$$

$$\overline{\mu}_{41} = \mu^*_{41} = 1 - \frac{C_p}{C_v}\left(i\nu + \frac{1}{2}\right), \tag{42}$$

$$\overline{\mu}_{42} = -\frac{C_p}{C_v}\left(i\nu + \frac{1}{2}\right)\frac{T^*}{\overline{T}}, \qquad \mu^*_{42} = -\frac{C_p}{C_v}\left(i\nu + \frac{1}{2}\right). \tag{43}$$

For the stability analysis, the growth of any mode with the shape function f is examined. The analysis hence consists in solving (12) assuming $\mathcal{X}_{(t=-\Delta t)} = \hat{\mathcal{X}}^-$, $f(x, \sigma)$ together with

$$\mathcal{X}_{(t=0)} = \lambda \mathcal{X}_{(t=-\Delta t)}, \tag{44}$$

$$\mathcal{X}_{(t=\Delta t)} = \lambda^2 \mathcal{X}_{(t=-\Delta t)}, \tag{45}$$

where the unknowns are the complex polarization vector $\hat{\mathcal{X}}^-$ and the numerical complex growth rate λ. As stated in B03, the 3-TL SI scheme is a particular ICI scheme with $N_{\text{iter}} = 1$ and $\mu(\lambda) = 2 - 1/\lambda$. Hence, in the formalism of B03, the stability problem reduces to

$$\begin{bmatrix} (2\lambda - 1)I_4 & -I_4 & 0_4 \\ M_1 & M_2 & M_3 \\ -\lambda^2 I_4 & 0_4 & I_4 \end{bmatrix} \mathcal{Z} = \mathbf{M}\mathcal{Z} = 0, \tag{46}$$

where the generalized state vector $\mathcal{Z}$ is defined by $\mathcal{Z} = [\hat{\mathcal{X}}^-, \hat{\mathcal{X}}^{+(0)}, \hat{\mathcal{X}}^{+(1)}]$, and I_4 and 0_4 are the unit and null fourth-order matrices, respectively. In the 3-TL SI framework, the submatrices M_1, M_2 and M_3 are defined by

$$(M_1)_{ij} = -\delta_{ij} - \Delta t\frac{\overline{\mu}_{ij}}{\xi_i}, \tag{47}$$

$$(M_2)_{ij} = -\Delta t\frac{1}{\xi_i}(\overline{\mu}_{ij} - \mu^*_{ij}), \tag{48}$$

$$(M_3)_{ij} = +\delta_{ij} - \Delta t\frac{\mu^*_{ij}}{\xi_i}, \tag{49}$$

where all notations follow B03. The possible values of λ for the normal-mode structure that we examine are thus given by the roots of the following polynomial equation in λ:

$$\text{Det}(\mathbf{M}) = 0. \tag{50}$$

In this simple case, the determinant is easily expanded algebraically and yields

$$\frac{(\Lambda_-)^4}{\Delta t^4} + c^2\frac{(\Lambda_-)^2}{\Delta t^2}(\Lambda_+)(k^2\tilde{\Lambda} + n\overline{n}\tilde{\tilde{\Lambda}}) + k^2N^2c^2(\Lambda_+)^2 \times \left\{\left[\frac{\tilde{\Lambda}\tilde{\tilde{\Lambda}}C_p - (\Lambda_+)^2 R}{C_v}\right] - nH[\tilde{\Lambda}\tilde{\tilde{\Lambda}} - (\Lambda_+)^2]\right\} = 0, \tag{51}$$

where the time-discretized response factors are defined by

$$\Lambda_- = \frac{\lambda^2 - 1}{2}, \tag{52}$$

$$\Lambda_+ = \frac{\lambda^2 + 1}{2}, \tag{53}$$

$$\tilde{\Lambda} = (\Lambda_+) + \alpha\lambda, \tag{54}$$

$$\tilde{\tilde{\Lambda}} = (\Lambda_+) - \frac{\alpha}{1+\alpha}\lambda, \quad \text{and} \tag{55}$$

$$\alpha = \frac{\overline{T} - T^*}{T^*}, \tag{56}$$

$$c^2 = RT^*(C_p/C_v), \tag{57}$$

$$H = RT^*/g, \tag{58}$$

$$N = g/\sqrt{C_p T^*}, \tag{59}$$

$$n = (i\nu + 1/2)H^{-1}, \tag{60}$$

$$\overline{n} = (-i\nu + 1/2)H^{-1}. \tag{61}$$

This eighth-degree complex polynomial equation in λ can be solved numerically: for any pair (k, ν), the modulus of the eight roots λ give the growth rate of the eight corresponding eigenmodes (four physical modes and four computational modes, due to the 3-TL discretization). If one of the roots has a modulus larger than one, then the corresponding mode is unstable. The stability of the scheme for the structure function f corresponding to a pair (k, ν) is then given by the maximum modulus of the eight corresponding eigenvalues:

$$\Gamma = \text{Max}(|\lambda_i|), \qquad i \in (1, \ldots, 8). \tag{62}$$

The criterion for ''asymptotic'' stability of the scheme with respect to the time step can be found by requiring stability at the large time steps' limit in the above equation. The terms containing Λ_- are then vanishing, and the equation for the growth rate becomes

$$(\Lambda_+)^2\left\{\tilde{\Lambda}\tilde{\tilde{\Lambda}}\frac{C_p}{C_v} - (\Lambda_+)^2\frac{R}{C_v} - nH[\tilde{\Lambda}\tilde{\tilde{\Lambda}} - (\Lambda_+)^2]\right\} = 0. \tag{63}$$

The four modes represented by $(\Lambda_+)^2 = 0$ are always neutral. Conversely, in the other set of roots the short vertical modes are always unstable. In effect, for these roots, substituting the time discretization response factors by their value leads to

$$(1+\alpha)(\lambda^2+1)^2 - 2\alpha^2\lambda(\lambda-1)^2 \times [i\nu + (1/2 - C_p/C_v)] = 0. \tag{64}$$

For short modes, $\nu \gg 1$; hence, the modulus of the four roots becomes close to

$$|\lambda|_{(1,2,3,4)} \approx \frac{2\alpha^2}{1+\alpha}\nu, \tag{65}$$

and obviously this leads to large instabilities. As a consequence, except in the degenerated case $\alpha = 0$, the scheme cannot be asymptotically stable in Δt, because for large time steps, short enough vertical modes are unstable.

However, drawing on the results of the previous section, the sensitivity of the stability to the choice of the prognostic variables is suspected, and the relevance of the original choice $\hat{d}$ could be questioned. A close inspection of the algebra in the above analysis indicates that the source of the problem lies in the small discrepancy between the $\tilde{\Lambda}\tilde{\tilde{\Lambda}}$ and $(\Lambda_+)^2$ in (63), which in turn is linked to the discrepancy between the D and $\hat{d}$ factors in the rhs of (29). This suggests the use of an alternative variable d that would be defined in the general hybrid coordinate η by

$$\text{d} = -g\frac{p}{mRT}\frac{\partial w}{\partial \eta}, \tag{66}$$

where $m = (\partial\pi/\partial\eta)$. In the present linear and hydrostatically balanced context with σ coordinate, d simplifies to

$$\text{d} = -g\frac{\sigma}{R\overline{T}}\frac{\partial w}{\partial \sigma}, \tag{67}$$

and the linear three-dimensional divergence writes

$$D_3 = D + \text{d}. \tag{68}$$

The linear system $\overline{\mathcal{L}}$ becomes

$$\frac{\partial D}{\partial t} = -R\mathcal{G}\nabla^2 T + R\overline{T}(\mathcal{G} - \mathcal{I})\nabla^2\mathcal{P} - R\overline{T}\nabla^2 q, \tag{69}$$

$$\frac{\partial \text{d}}{\partial t} = -\frac{g^2}{R\overline{T}}\tilde{\partial}(\tilde{\partial} + \mathcal{I})\mathcal{P}, \tag{70}$$

$$\frac{\partial T}{\partial t} = -\frac{R\overline{T}}{C_v}(D + \text{d}), \tag{71}$$

$$\frac{\partial \mathcal{P}}{\partial t} = \mathcal{S}D - \frac{C_p}{C_v}(D + \text{d}), \tag{72}$$

$$\frac{\partial q}{\partial t} = -\mathcal{N}D. \tag{73}$$

Since $\hat{d}$ and d have the same value in the SI reference state, the general design of the SI scheme is unchanged. The linear system $\mathcal{L}^*$ is formally identical to the previous one; hence, the modification does not change the SI equation to be solved. The stability analysis for this new system can be done exactly in the same way as presented above, and the stability equation (51) for a given geometry (k, ν) becomes

$$\frac{(\Lambda_-)^4}{\Delta t^4} + c^2\frac{(\Lambda_-)^2}{\Delta t^2}(\Lambda_+)(k^2\tilde{\Lambda} + n\overline{n}\tilde{\tilde{\Lambda}}) + k^2N^2c^2(\Lambda_+)^2\tilde{\Lambda}\tilde{\tilde{\Lambda}} = 0. \tag{74}$$

As previously, the asymptotic stability in Δt can be examined by neglecting all terms containing Λ_-, and the numerical growth rate is then given by

$$(\lambda^2+1)^2(\lambda^2+1+2\alpha\lambda)\left(\lambda^2 + 1 - 2\frac{\alpha}{1+\alpha}\lambda\right) = 0. \tag{75}$$

The four modes involved by the first factor are always neutral. Basic algebraic manipulations show that the modes involved in the second factor are stable for $-1 \leq \alpha \leq 1$, while the last factor requires $-1/2 \leq \alpha$ for stability. Finally, considering the definition of α, the scheme is asymptotically stable in Δt when the following condition is fulfilled:

$$\frac{T^*}{2} \leq \overline{T} \leq 2T^*. \tag{76}$$

The above type of stability analyses can be performed in the same way for any other vertical-velocity-related prognostic variable. From the set $\{w, (\partial w/\partial \eta), \hat{d}, \mathrm{d}\}$, only the last variable is then found to allow a nonvanishing range of asymptotic stability in mass-based coordinates. But conversely to what occurred in the previous section, this result is now dependent on the type of vertical coordinate used: for height-based coordinates, the same kind of analysis (see appendix B) shows that the two most natural choices $\{w, \partial w/\partial z\}$ lead to the same asymptotic stability criterion than one obtained here for the d variable in mass-based coordinates. Hence, from the point of view of the asymptotic stability at long time steps, both height- and mass-based coordinates behave identically provided ''optimal'' variables are chosen. The fact that d in mass-based coordinates and $(\partial w/\partial z)$ in height-based coordinates behave similarly can be understood intuitively since these two variables are in fact two expressions of a same concept in the present simplified context (i.e., they both represent the true vertical divergence here). The reason why w is stable in height-based coordinates but unstable in mass-based coordinates is more subtle: as suggested by the above analyses, the robustness of the SI scheme appears to be highly correlated to the existence of NL residuals in the elastic term D_3; when w is used as a prognostic variable in height-based coordinates, D_3 can be readily obtained from $D + (\partial w/\partial z)$ and has no NL residual, thus leading to a stable scheme in the examined context. With mass-based coordinates, however, if w is chosen as a prognostic variable, D_3 must be evaluated through $D - (gp/RT)(\partial w/\partial \pi)$ and the existence of an NL residual when $T \neq T^*$ may lead to instabilities. The fact that the vertical divergence d is completely imposed as a prognostic variable if a robust SI scheme is desired for the EE system with flat terrain is thus a specificity of mass-based coordinates.

Another important result from the above analysis is that, even with an optimal choice of the prognostic variables, the stability range is dramatically reduced for the EE system compared to the HPE system, whatever vertical coordinate is used. For HPEs (see, e.g., SHB78), the criterion (76) would write

$$0 \leq \overline{T} \leq 2T^*. \tag{77}$$

Choosing a very warm T^* guarantees stability in HPEs while this is no longer the case for EEs. Moreover, if the actual temperature were to vary by more than a factor 4 in the atmosphere, the SI technique examined here could not offer any stable scheme for the EE system. The SI EE system is thus less stable *by nature* than the SI HPE system, and its applicability for NWP is only made possible thanks to the moderate variability of the thermal field in the terrestrial atmosphere.

5. Practical implications

For a given mode, the root of maximum modulus in (64) and (75) gives the asymptotic growth rate for large time steps for the two variables $\hat{d}$ and d examined above. For the variable $\hat{d}$, this asymptotic growth rate is a function of α and ν; hence, the instability is directly linked to the vertical resolution of the model. For the variable d the asymptotic growth rate is a function of α only. Figure 1 shows the asymptotic growth rate for a vertical spacing of 100 m (i.e., a minimum vertical wavelength of 200 m), for $\hat{d}$ and d, in the conditions of the above analyses. Assuming a typical value ± 0.25 for α in realistic conditions, the range of growth rate for the variable $\hat{d}$ is clearly incompatible with a stable integration of the SI scheme with very long time steps. In practical applications, however, the time step is bounded, and the growth, if present, may not endanger significantly the stability of the scheme. However, direct numerical solution of (51) shows that in fact any mode (k, ν) is unstable for any time step, when $\alpha \neq 0$. For instance, also plotted in Fig. 1 are the numerical growth rates obtained for a mode whose geometry is close to the shortest mode for a typical mesoscale future NWP limited-area target configuration with 3-TL semi-Lagrangian scheme ($\Delta x = 2000$ m, $\Delta z = 100$ m, and $\Delta t = 20$ s): the system with $\hat{d}$ variable is significantly unstable as soon as $\alpha \neq 0$, even for this modest time step. The $\hat{d}$ variable is clearly demonstrated as not suitable for use in a SI EE scheme in mass-based coordinates. This was one of the reasons why an iterative procedure was required and applied in the NH model described in BHBG95.

An additional remark concerning the stability for finite time steps is that, surprisingly, when an optimal variable is chosen in height-based coordinates, the SI scheme, which is stable for long time steps, becomes slightly unstable for finite time steps as soon as $\alpha \neq 0$, as seen in appendix B. A similar behavior was found in B03 for the one-dimensional acoustic system with long time steps in height-based coordinates. This unstable behavior can be interpreted as originating from the fact that in height-based coordinates, the time-continuous normal modes of the $\mathcal{L}$ system are not normal modes of $\mathcal{L}^*$, as pointed out in appendix B. As a consequence, the time-continuous evolution of any normal mode of $\mathcal{L}$ by the $\mathcal{L}^*$ system contains a growing component (i.e., a complex nonreal frequency) as soon as $\alpha \neq 0$. The SI scheme is then not able to ensure a stable evolution for some of these components. This type of instability does not occur for mass-based coordinates,

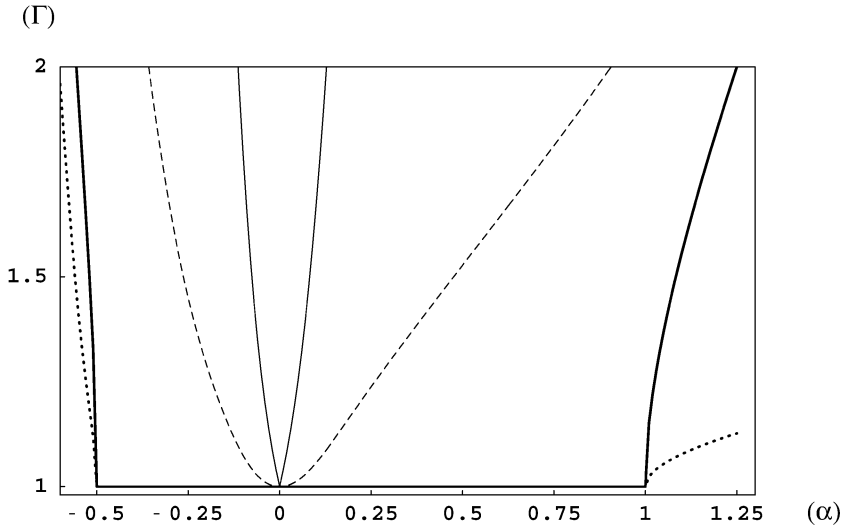

FIG. 1. Analytic growth rates (GR) for the simplified problem as a function of the nonlinearity parameter α. The thick line is the asymptotic GR for variable d; solid line, asymptotic GR for variable $\hat{d}$; dotted line, practical GR for variable d; dashed line, practical GR for variable $\hat{d}$ (see text for the meaning of practical GR).

as seen in Fig. 1. From the theoretical point of view, this behavior pleads in favor of mass-based coordinates, but it should be noted that the resulting instabilities are generally moderate (not shown) and could be controlled by the use of slightly damping algorithms [e.g., SI decentering as in Laprise et al. (1997)] or by the diffusive processes acting in a complete model.

The stability of the SI scheme can be studied for nonisothermal linear atmospheric flows, using the ''numerical analysis'' method proposed by CBS83: The linearized equations have first to be vertically discretized. For a given eigenmode of the horizontal ∇^2 operator, the actual and reference model operators can then be expressed as two matrices $\overline{\mathbf{L}}$ and $\mathbf{L}^*$ operating on the perturbation state vector $\mathbf{X}$. The equation of model evolution (12) then writes

$$\mathbf{Y}^{t+\Delta t} = \mathbf{A} \cdot \mathbf{Y}^t, \tag{78}$$

where the generalized state vector $\mathbf{Y}^t$ is defined by ($\mathbf{X}^t$, $\mathbf{X}^{t-\Delta t}$), and the amplification matrix $\mathbf{A}$ is given by

$$\mathbf{A} = \begin{bmatrix} 2\Delta t(\mathbf{I}_X - \Delta t\mathbf{L}^*)^{-1} \cdot (\overline{\mathbf{L}} - \mathbf{L}^*) & (\mathbf{I}_X - \Delta t\mathbf{L}^*)^{-1} \cdot (\mathbf{I}_X + \Delta t\mathbf{L}^*) \\ \mathbf{I}_X & \mathbf{0}_X \end{bmatrix}, \tag{79}$$

where $\mathbf{I}_X$ and $\mathbf{0}_X$ are the identity and null operators in the state-vector space, respectively. Noting Γ, the largest modulus of $\mathbf{A}$ eigenvalues, the scheme is stable if $\Gamma \leq 1$ and unstable if $\Gamma > 1$. The eigenvector associated with Γ gives the vertical structure and polarization of the most unstable mode.

Our implementation of this ''numerical analysis'' method has been validated by comparison with the results of the above analyses: the agreement was found to be very good (not shown). Here, the ''numerical analysis'' method is applied to quantify the impact of the change from $\hat{d}$ to d in more realistic situations than the one assumed in the above analyses. Following SHB78, a realistic actual temperature profile is chosen: it consists in a tropospheric profile with a quasi-uniform dry static stability and an isothermal stratosphere above 200 hPa, as depicted in Fig. 2 (the surface temperature is set to 285 K). The vertical discretization of $\overline{\mathcal{L}}$ and $\mathcal{L}^*$ models follows BHBG95. The numerical analysis is performed for the same typical future NWP target values for (Δx, Δt) as in Fig. 1. The stability is examined for values of T^* varying in the interval [200 K, 320 K].

Figure 2 shows the growth rates obtained for 10, 20, and 30 regularly spaced σ levels, for the $\hat{d}$ and d variables. The theoretical disadvantage of $\hat{d}$ is confirmed: for high vertical resolutions, the scheme is unstable for almost every value of T^*, with growth rates uncompatible with a practical use. The logarithm of the growth rate is found to be roughly proportional to the horizontal wavenumber k, confirming that troubles linked to the presence of NL terms become more and more stringent when the horizontal resolution is increased. Moreover, reducing the time step is found to be of no help for a given forecast range because the logarithm of the growth

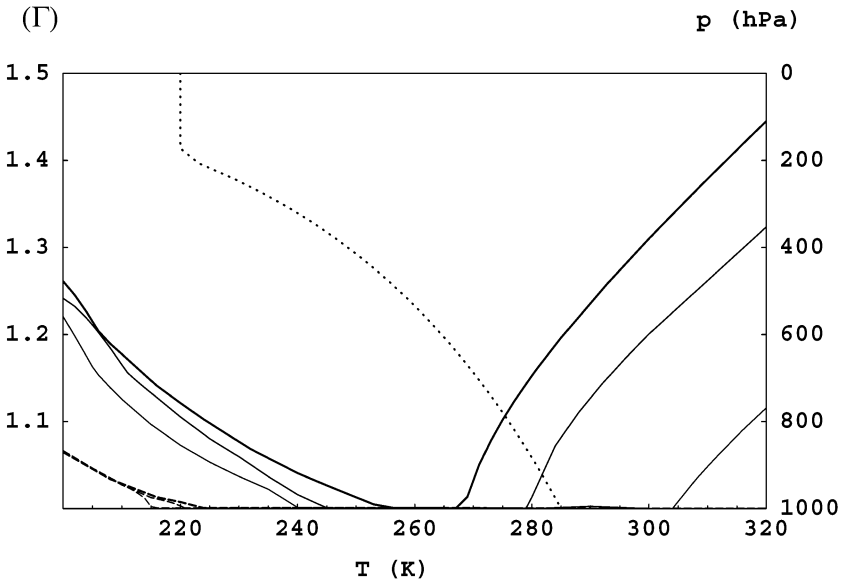

FIG. 2. Numerical growth rate (left axis) for the realistic thermal profile (dotted line, with pressure indicated on right axis), as a function of T^*. From thin to thick lines: 10, 20, 30 levels. Solid line is variable $\hat{d}$, and dashed line is variable d.

rate is always roughly proportional to the time step. Conversely, the use of variable d results in a stable scheme provided T^* is chosen to be warm enough in the examined interval (and up to 440 K here, consistently with analyses).

Taking d as a prognostic variable, the impact of the choice of the nonhydrostatic pressure variable ($\hat{\mathcal{P}}$ versus $\mathcal{P}$) can be examined numerically, still in the same context. It has been shown in section 3 why the system could be potentially unstable when $\overline{\pi}_s$ deviates from π_s^*. To confirm and illustrate this statement, two values of π_s^* are chosen (813.25 and 1213.25 hPa), while $\overline{\pi}_s$ is assumed to be 1013.25 hPa, still for the same thermal profile and experimental context as above, and for 30 regularly spaced σ levels. The solid lines in Fig. 3 show the growth rates obtained for the variable $\hat{\mathcal{P}}$ (as explained in section 3, the growth rate has no dependency on π_s^* when the variable $\mathcal{P}$ is used; hence, the correspond-

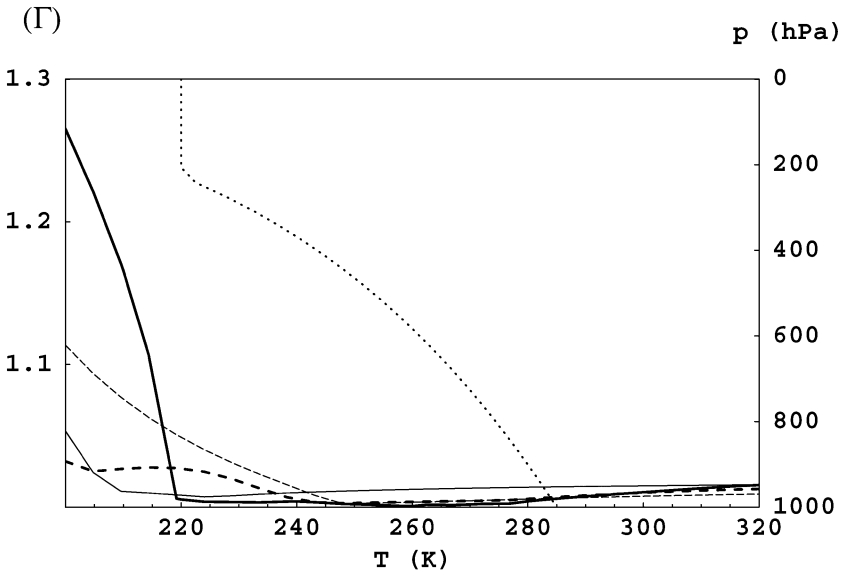

FIG. 3. Numerical growth rate (left axis) for the realistic thermal profile (dotted line, with pressure indicated on right axis), as a function of T^*. Thick lines: $\pi_s^* = 1213.25$ hPa; thin lines: $\pi_s^* = 813.25$ hPa; solid line: variable $\hat{\mathcal{P}}$ with σ coordinate; dashed line: variable $\mathcal{P}$ with η coordinate.

ing growth rate for the variable $\mathcal{P}$ can be seen in Fig. 2, regardless of the value of π_s^*). The use of the $\hat{\mathcal{P}}$ variable induces a global decrease in stability especially for $\pi_s^* = 1213.25$ hPa and low values of T^*. For high values of T^*, an instability subsists for both values of π_s^*, but it is weak (growth rates around 1.015), and the practical risk of using $\hat{\mathcal{P}}$ for NWP is hence difficult to assess from this simplified theory and should be evaluated in a more realistic context. However, since there is no other potential advantage of using $\hat{\mathcal{P}}$ instead of $\mathcal{P}$, this question is probably not of primary interest.

Finally, examination of the above algebra shows that the hybrid η coordinate can also be responsible for instabilities when $\overline{\pi}_s$ deviates from π_s^*, as it may, for example, be the case when the terrain is uniformly elevated. This is linked to the fact that in η coordinate, all vertical operators ($\mathcal{G}$, $\mathcal{S}$, $\mathcal{N}$, $\tilde{\partial}$) deviate from their SI reference counterpart when $\overline{\pi}_s \neq \pi_s^*$, the resulting NL residuals potentially leading to instability. The discrepancy between the vertical metrics of $\overline{\mathcal{L}}$ and $\mathcal{L}^*$ models makes impossible the analysis for a general choice of A and B functions; hence, we use the ''numerical analysis'' method proposed by CBS83 to examine the impact of using a hybrid coordinate instead of a pure terrain-following coordinate when $\overline{\pi}_s \neq \pi_s^*$.

The dashed lines in Fig. 3 show the growth rates obtained for the variable $\mathcal{P}$ when a regularly flattening unstretched η coordinate, defined by $\pi(\eta) = -\rho\eta \ln(\eta)p_{00} + \eta[1 + \rho \ln(\eta)]\pi_s$ (with $p_{00} = 1013.25$ hPa, and $\rho = 0.25$) is used with the same realistic thermal profile and discrepancies of ± 200 hPa between $\overline{\pi}_s$ and π_s^* as above. For high values of T^*, the loss of stability is of similar magnitude as the one resulting from the choice of $\hat{\mathcal{P}}$ as prognostic variable. It is noteworthy that the instability linked to the use of the hybrid coordinate in EE cannot be eliminated by choosing high values for T^*, as was the case for the HPE system (Simmons and Temperton 1997); hence, there is indication that the hybrid η coordinate possesses a slight theoretical disadvantage from this point of view, but this may be not redhibitory in practice. In other respects, it has been claimed that the η coordinate brings some advantages compared to σ coordinates, especially for the accuracy of the pressure-gradient force computation and for the assimilation of high-level data (Simmons and Burridge 1981). Hence, according to the warning signal obtained here, the question of the relevance of the hybrid coordinate should legitimately have to be considered when implementing a real-case application in the EE system with π-type coordinate but cannot be answered with a reasonable certainty at this stage.

6. Comments

The intrinsic sensitivity of SI schemes' stability to the choice of prognostic variables, which has been demonstrated in this paper, is totally independent of the space discretization, since the analyses have been performed in the space-continuous context. As a consequence, any numerical model built with an intrinsically unstable variable will exhibit an unstable behavior, regardless of the space-discretization and staggering choices that may be done. However, it has been shown that an intrisincally stable variable for height-based coordinates can become intrinsically unstable for mass-based coordinates because of the flow-dependent vertical metrics of this type of coordinate. Hence, it appears that for designing an SI numerical model in the EE system, the choice of the prognostic variables cannot be made independently of the choice of the vertical coordinate, even at the level of space-continuous equations.

One could wonder if this dependency is specific to the EE system or if it was already present in HPE systems, which are cast in π-type coordinates. First it should be noted that the HPE system does not offer a large latitude for the choice of prognostic variables: for the problems examined here, the prognostic variable for the vertically integrated continuity equation is the only relevant one: it can be set to be π_s or $q = \ln(\pi_s)$. The above numerical method applied to the HPE system demonstrates the absence of sensitivity to the choice of these prognostic variables (not shown). For instance, the instabilities reported by Simmons and Temperton (1997), which are the consequence of using a hybrid coordinate, develop almost identically for π_s and $q = \ln(\pi_s)$ variables. The sensitivity of the stability to the choice of the set of prognostic variables discussed here is thus a specificity of fully elastic nonhydrostatic systems (anelastic systems have not been examined).

7. Conclusions

The stability of constant-coefficients SI schemes for the system of Euler equations has been examined from a theoretical point of view, in deliberately simplified contexts to allow tractable analyses. The salient result of the study is that the stability can be dramatically affected by changes in the set of prognostic variables that are used to design the SI scheme, and this, independently of any space discretization. It appears that the choice of the two ''nonhydrostatic'' variables has to be carefully checked if an optimal stability is desired, especially for mass-based coordinates. Nonoptimal choices generally result in growth rates incompatible with a practical NWP use, as experienced in BHBG95. This sensitivity of the SI scheme stability to the choice of prognostic variables was not present in the HPE system.

If the SI reference surface pressure deviates from its actual counterpart for mass-based coordinates, hybrid coordinates are found more unstable than the corresponding pure terrain-following coordinates, as reported previously for the HPE system, but the practical consequences of this slight instability need to be evaluated in more realistic contexts.

The analyses and results reported in this paper apply

to constant-coefficients SI schemes; however, since only thermal and baric NL residuals are involved, the results extend identically to those SI schemes belonging to class (ii) of the introduction, for which the reference temperature and pressure are horizontally homogeneous (e.g., Thomas et al. 1998; Qian et al. 1998).

The practical interest of this theoretical study could be considered quite limited, since only a very small part of the NL terms due to the discrepancy between the actual state $\mathcal{X}$ and the SI reference state $\mathcal{X}^*$ has been considered. In this respect, the developments presented here should rather be viewed as an endeavor to stress that a special care must be exerted in the choice of prognostic variables for building a constant-coefficients SI EE system, whatever type of coordinate is used.

In a more general way, there is another practical interest to this study: as a predictive tool, it can serve for the validation of practical numerical applications. In a similar way that analytically predicted stationary orographic flows are commonly used for validating the relevance of space-discretization schemes, the analytically predicted stability can be used for a careful validation of time-discretization schemes. Moreover, if a ''numerical analysis'' tool is built, a complete set of cross-validations becomes possible between analyses predictions, numerical-analyses diagnostics, and observed numerical-model behavior. This may significantly help to improve the detection of anomalous behavior in a numerical model or the prediction of the behavior of alternative time discretizations (off-centered SI scheme, iterative treatments, etc.).

Nevertheless, as stated above, this study unavoidably leads to an overestimation of the stability in comparison to the likely stability for real-case conditions because it retains only a very small part of all NL terms arising from the discrepancy ($\mathcal{M} - \mathcal{L}^*$). Among the most important sources of NL residuals, the spatial variability of the orography has been neglected so far. Hence, there is no proof that the optimal set found here (e.g., q, $\mathcal{P}$, d, and σ coordinate) is still optimal, or even reasonnably stable, when a steep orography is introduced. Further examination of this topic would constitute an interesting extension of the present study.

Acknowledgments. Part of the research reported in this paper was supported by the ALATNET Grant HPRN-CT-1999-00057 of the European Union TMR/IHP Programme. The authors would like to thank Dr. Claude Girard for fruitful discussions and for the experimental confirmation of the analytical results of appendix B as well as an anonymous reviewer for his helpful comments.

APPENDIX A

List of Symbols

Space-continuous version of vertical operators in σ coordinate

$$\mathcal{G}X = \int_\sigma^1 \left(\frac{X}{\sigma'}\right) d\sigma'$$

$$\mathcal{S}X = \left(\frac{1}{\sigma}\right) \int_0^\sigma X \, d\sigma'$$

$$\mathcal{N}X = \int_0^1 X \, d\sigma$$

$$\mathcal{I}X = X$$

$$\tilde{\partial}X = \sigma(\partial/\partial\sigma)X.$$

Miscellaneous symbols

$\boldsymbol{\nabla}$	Horizontal gradient operator along constant surfaces of the considered vertical coordinate
$\mathbf{V}$	Horizontal wind vector in 3D framework
∇	$(\partial/\partial x)$ along constant levels of the considered vertical coordinate in the 2D vertical-plane domain
$(\partial/\partial t)$	Eulerian time derivative
(d/dt)	Lagrangian time derivative
D	Horizontal wind divergence (∇u)
g	Gravitational acceleration
p	True pressure
π	Hydrostatic pressure
p_{00}	Absolute reference pressure (1013.25 hPa)
R, C_p, C_v	Dry air thermodynamic constants
T	Temperature
u	Horizontal wind component in the 2D framework

APPENDIX B

Stability Analysis of the EE in Regular Gal-Chen Coordinate

The formalism for the derivation of the constant-coefficients SI scheme analyzed here basically follows Caya and Laprise (1999). Notations are standard ones and are taken identical to this paper unless specified. The unstretched Gal-Chen coordinate is defined by

$$\zeta = \frac{z - h_0}{H_D - h_0} H_D, \tag{B1}$$

where H_D is the height of the domain, and h_0 is the height of the terrain. In the absence of orography ($h_0 \equiv 0$) we thus have

$$\zeta = z. \tag{B2}$$

The general framework is the same as in the above analyses, as depicted in section 2, and the thermal discrepancy between $\overline{\mathcal{X}}$ and $\mathcal{X}^*$ states is still noted $\alpha = (\overline{T} - T^*)/T^*$. However, unlike for mass-based coordinates, the pressure variable $q = \ln(p/p_{00})$ [not to be

confused with $q = \ln(\pi_s)$ for mass-coordinates systems in the main part of the paper] needs to be defined in the whole space for both $\overline{\mathcal{X}}$ and $\mathcal{X}^*$ states. The hydrostatic equilibrium and stationarity of these states implies

$$\overline{T}\frac{d\overline{q}}{dz} = T^*\frac{dq^*}{dz} = -\frac{g}{R}. \tag{B3}$$

The SI time-discretized system is given by Eqs. (46)–(50) of Caya and Laprise (1999):

$$\frac{du}{dt} + RT^*\overline{\nabla q'}^t = -RT'\nabla q', \tag{B4}$$

$$\frac{dw}{dt} + RT^*\frac{\overline{\partial q'}^t}{\partial z} - \frac{g}{T^*}\overline{T'}^t = -RT'\frac{\partial q'}{\partial z}, \tag{B5}$$

$$\frac{dT'}{dt} - \frac{RT^*}{C_p}\frac{dq'}{dt} + \frac{g}{C_p}\overline{w}^t = -\frac{R}{C_v}T'\left(\nabla u + \frac{\partial w}{\partial z}\right), \tag{B6}$$

$$\frac{C_v}{C_p}\left(\frac{dq'}{dt} - \frac{g}{RT^*}\overline{w}^t\right) + \left(\overline{\nabla u}^t + \frac{\overline{\partial w}^t}{\partial z}\right) = 0, \tag{B7}$$

where $T' = T - T^*$ and $q' = q - q^*$. This system is exact in the sense that no term has been neglected so far. As can be seen from the notation $\overline{\ }^t$, the left-hand sides are treated in a centered implicit way while the right-hand sides are treated explicitly. For the analysis, a small pertubation $(\tilde{T}, \tilde{q})$ around the actual state $(\overline{T}, \overline{q})$ must be introduced, and the complete system must be linearized around $(\overline{T}, \overline{q})$. Equating the total variables T and q yields

$$\tilde{T} = T' - \alpha T^*, \tag{B8}$$

$$\tilde{q} = q' - \frac{\alpha}{(1+\alpha)}\frac{g}{RT^*}z. \tag{B9}$$

The terms that are nonlinear in $(u, w, \tilde{T}, \tilde{q})$ are then dropped in the above system (T' and q' cannot be considered as small, however). The actual state $\overline{\mathcal{X}}$ being a resting state, time derivatives are replaced by $(\partial/\partial t)$. However, a special care must be taken to express (dq'/dt) in term of $(d\tilde{q}/dt)$, because the vertical transport of $(\overline{q} - q^*)$ is a linear term that must be retained. If an Eulerian scheme for the vertical advection is used, then

$$\frac{\partial q'}{\partial t} = \frac{\partial \tilde{q}}{\partial t} + \frac{\alpha}{1+\alpha}\frac{g}{RT^*}w, \tag{B10}$$

where the advection term is treated explicitly. For a semi-Lagrangian vertical transport scheme, the assumptions of perfect solution for the displacement equation, and of perfect interpolators, consistent with the space-continuous context, lead after some manipulation based on Taylor series expansions in space, to the same result as for the Eulerian advection scheme as written in (B10).

The linearization of the above system around the $\overline{\mathcal{X}}$ state leads to, after some algebraic manipulation, a form compatible with the analysis proposed in B03. The $\overline{\mathcal{L}}$ system then writes

$$\frac{\partial u}{\partial t} = -R\overline{T}\nabla\tilde{q}, \tag{B11}$$

$$\frac{\partial w}{\partial t} = \frac{g}{\overline{\overline{T}}}\tilde{T} - R\overline{T}\frac{\partial \tilde{q}}{\partial z}, \tag{B12}$$

$$\frac{\partial \tilde{q}}{\partial t} = \frac{g}{R\overline{T}}w - \frac{C_p}{C_v}\left(\nabla u + \frac{\partial w}{\partial z}\right), \tag{B13}$$

$$\frac{\partial \tilde{T}}{\partial t} = -\frac{R\overline{T}}{C_v}\left(\nabla u + \frac{\partial w}{\partial z}\right). \tag{B14}$$

The SI reference system $\mathcal{L}^*$ is shown to be formally identical, but with $\overline{T}$ replaced by T^*. We have $P = 4$, and the normal modes of the time-continuous system are given by

$$\mathcal{X}_j(x, z) = \hat{\mathcal{X}}_j \exp(ikx)\exp(nz) \qquad j \in (1, \ldots, 4), \tag{B15}$$

where $n = (i\nu + 1/2)/\overline{H}$, and $\overline{H} = R\overline{T}/g$. It should be noted that the time-continuous normal modes of the $\mathcal{L}^*$ system have a different vertical structure $\exp(n^*z)$, with $n^* = (i\nu + 1/2)g/(RT^*)$. This discrepancy between the height scales for the vertical growth of $\overline{\mathcal{L}}$ and $\mathcal{L}^*$ time-continuous normal modes has some important consequences, as discussed in section 5.

The analysis then proceeds as for mass-based coordinates by defining a numerical growth rate λ. For a given geometry (k, ν), the stability equation finally writes

$$\frac{(\Lambda_-)^4}{\Delta t^4} + \frac{(\Lambda_-)^2}{\Delta t^2}c^2\left[k^2(\Lambda_+)\tilde{\Lambda} + n\overline{n}(\Lambda_+)\tilde{\Lambda} + n\tilde{\Lambda}\frac{\alpha}{\overline{\overline{H}}}(\Lambda_+ - \lambda)\right] + k^2N^2c^2\tilde{\Lambda}^2\tilde{\tilde{\Lambda}}^2 = 0, \tag{B16}$$

where Λ_-, Λ_+, $\tilde{\Lambda}$, $\tilde{\tilde{\Lambda}}$, c, H, N are defined as in (52)–(59).

The asymptotic growth rate is then given by the same equation [(75)] as for mass-based coordinates; hence, the conditions for asymptotic stability are the same as well. However, a major difference between Eqs. (B16) and (74) is the presence of the last complex term in the bracket of (B16). The solution of this equation for finite time steps shows that this term, being complex, is responsible for an instability when $\alpha \neq 0$. The instability is generally small but is found to become quite significant when $k\overline{H} \approx \nu \approx 1$, but, as stated above, it always disappears for long time steps.

REFERENCES

Bénard, P., 2003: Stability of semi-implicit and iterative centered-implicit time discretizations for various equation systems used in NWP. *Mon. Wea. Rev.*, **131,** 2479–2491.

Bubnová, R., G. Hello, P. Bénard, and J. F. Geleyn, 1995: Integration of the fully elastic equations cast in the hydrostatic pressure terrain-following coordinate in the framework of the ARPEGE/Aladin NWP system. *Mon. Wea. Rev.*, **123,** 515–535.

Caya, D., and R. Laprise, 1999: A semi-implicit semi-Lagrangian regional climate model: The Canadian RCM. *Mon. Wea. Rev.*, **127,** 341–362.

Côté, J., M. Béland, and A. Staniforth, 1983: Stability of vertical discretization schemes for semi-implicit primitive equation models: Theory and application. *Mon. Wea. Rev.,* **111,** 1189–1207.

Laprise, R., 1992: The Euler equations of motion with hydrostatic pressure as an independent variable. *Mon. Wea. Rev.,* **120,** 197–207.

——, D. Caya, G. Bergeron, and M. Giguère, 1997: The formulation of the André Robert MC2 (mesoscale compressible community) model. *Numerical Methods in Atmospheric Modeling,* C. Lin et al., Eds., Canadian Meteorological and Oceanographic Society, CMOS-NRC Research Press, 195–220.

Qian, J.-H., F. H. M. Semazzi, and J. S. Scroggs, 1998: A global nonhydrostatic semi-Lagrangian atmospheric model with orography. *Mon. Wea. Rev.,* **126,** 747–771.

Robert, A. J., J. Henderson, and C. Turnbull, 1972: An implicit time integration scheme for baroclinic models of the atmosphere. *Mon. Wea. Rev.,* **100,** 329–335.

Semazzi, F. H. M., J. H. Qian, and J. S. Scroggs, 1995: A global nonhydrostatic semi-Lagrangian atmospheric model without orography. *Mon. Wea. Rev.,* **123,** 2534–2550.

Simmons, A. J., and D. Burridge, 1981: An energy and angular-momentum conserving vertical finite-difference scheme and hybrid vertical coordinates. *Mon. Wea. Rev.,* **109,** 758–766.

——, and C. Temperton, 1997: Stability of a two-time-level semi-implicit integration scheme for gravity wave motion. *Mon. Wea. Rev.,* **125,** 600–615.

——, B. Hoskins, and D. Burridge, 1978: Stability of the semi-implicit method of time integration. *Mon. Wea. Rev.,* **106,** 405–412.

Tanguay, M., A. Robert, and R. Laprise, 1990: A semi-implicit semi-Lagrangian fully compressible regional forecast model. *Mon. Wea. Rev.,* **118,** 1970–1980.

Thomas, S. J., C. Girard, R. Benoit, M. Desgagné, and P. Pellerin, 1998: A new adiabatic kernel for the MC2 model. *Atmos.–Ocean,* **36,** 241–270.